ARTICLES

Journal of Semiconductors
(2022) 43, 052001
doi: 10.1088/1674-4926/43/5/052001

Magnetic tuning in a novel half-metallic Ir_2TeI_2 monolayer

Didi Zhao, Chenggong Zhang, Changwen Zhang, Weixiao Ji, Shengshi Li, and Peiji Wang†

School of Physics and Technology, Spintronics Institute, University of Jinan, Jinan 250022, China

Abstract: A two-dimensional (2D) high-temperature ferromagnetic half-metal whose magnetic and electronic properties can be flexibly tuned is required for the application of new spintronics devices. In this paper, we predict a stable Ir_2TeI_2 monolayer with half-metallicity by systematical first-principles calculations. Its ground state is found to exhibit inherent ferromagnetism and strong out-of-plane magnetic anisotropy of up to 1.024 meV per unit cell. The Curie temperature is estimated to be 293 K based on Monte Carlo simulation. Interestingly, a switch of magnetic axis between in-plane and out-of-plane is achievable under hole and electron doping, which allows for the effective control of spin injection/detection in such 2D systems. Furthermore, the employment of biaxial strain can realize the transition between ferromagnetic and antiferromagnetic states. These findings not only broaden the scope of 2D half-metal materials but they also provide an ideal platform for future applications of multifunctional spintronic devices.

Key words: two-dimensional materials; spintronics; half-metal; magnetic anisotropy energy

Citation: D D Zhao, C G Zhang, C W Zhang, W X Ji, S S Li, and P J Wang, Magnetic tuning in a novel half-metallic Ir_2TeI_2 monolayer[J]. *J. Semicond.*, 2022, 43(5), 052001. https://doi.org/10.1088/1674-4926/43/5/052001

1. Introduction

Two-dimensional (2D) magnets have become the subject of intensive research activities in condensed matter physics and material science thanks to their exciting and advanced properties, and potential applications in low dimensional spintronics devices. However, most intrinsic 2D materials are nonmagnetic and unfavorable for practical applications. At present, researchers have been devoted to exploring 2D van der Waals ferromagnetic (FM) materials, such as CrI_3[1], $Cr_2Ge_2Te_6$[2], Fe_3GeTe_2[3], VSe_2[4], $MnSe_2$[5], and $FePS_3$[6, 7]. These findings have triggered a surge of efforts to explore novel 2D transition metal compounds. Despite this effort, many challenges remain in this field of research, such as the presence of long-range ferromagnetic order and the considerable Curie temperature (T_c). According to the Mermin-Wagner theorem[8], the long-range magnetic order is prohibited in a 2D Heisenberg system, whereas it is available in a 2D Ising system. In contrast to a Heisenberg magnetic model, having a nonzero magnetic moment in only one direction is the dominant feature of uniaxial magnetic ions. In such a 2D system, the key to the stable existence of 2D long-range magnetic order at finite temperature is that magnetic anisotropy (MA) aligns their magnetic moments, canceling out thermal fluctuations[9–11]. Meanwhile, 2D ferromagnetic materials with T_c above room temperature are desirable to practical applications[12] but they are extremely rare. For example, the T_c of $Cr_2Ge_2Te_6$ bilayer and CrI_3 monolayer is demonstrated to be 28 and 45 K[1, 2], respectively, which is definitely lower than the ideal temperature and has restricted their application. To be brief, exploiting 2D ferromagnetic Ising system with large magnetic anisotropy energy (MAE) and high T_c is significantly important for the realization of a spintronic device with low energy consumption, high storage density, and high thermal stability[13–16].

Starting from the perspective of applications, precise and flexible control of the magnetic and electronic properties of 2D materials is a target that is always pursued[17–25]. So far, considerable efforts have been devoted to seeking for new 2D intrinsic magnetic materials, as well as to manipulate the magnetism using mechanical and electrical measures[26–31]. The magnetic properties of a material are generally associated with its structural parameters, which can be directly influenced by strain. Thus, the effective manipulation of magnetic properties is expected to be achieved by the strain engineering[32–36]. For instance, the T_c of $Cr_2Ge_2Se_6$ monolayers can be enhanced beyond room temperature by applying slight tensile strains[36]. Charge doping has been proved to tune the electrical and magnetic properties of 2D materials on a very wide scale and to drive electronic phase transitions[31, 37]. For instance, conversion of its magnetization intensity by electrostatic doping in a 2D CrI_3 film[38]. In addition, the transition from FM semiconductor to a half-metal and the tuning of MAE can be carried out by charge doping[39]. These results highlight the possibility of tuning magnetic properties in 2D ferromagnetic systems. In view of this, a 2D FM half-metal with controllable magnetism has great potential for highly efficient spintronic devices and non-volatile magnetic storage devices[40–43].

Here, we investigate a new 2D intrinsic FM Ir_2TeI_2 monolayer via first principles, which is magnetized out-of-plane and possesses large spin polarization, large MAE, and high T_c. Its magnetic control is relatively easy to be achieved by carrier injection, which can switch the magnetization axis between in-plane and out-of-plane directions. We find that biaxial strain can be used as a switch to achieve a stable switching between FM and antiferromagnetic (AFM) states. This behavior can be understood in terms of the competition between

Correspondence to: P J Wang, ss_wangpj@ujn.edu.cn
Received 5 NOVEMBER 2021; Revised 18 NOVEMBER 2021.

the direct exchange interaction and the super exchange interaction. In addition, the MAE increased under biaxial compression strain. This work provides a multifunctional 2D material and broadens its range.

2. Computational method

First-principles calculations are primarily carried out using the Vienna Ab initio Simulation Package (VASP)[44, 45], the exchange correlation function is treated under the generalized gradient approximation in the form proposed by Perdew–Burke–Ernzerhof (PBE)[46]. The GGA+U correction is employed (U = 3.0 eV) to cope with strongly correlated d electrons of Ir atoms[47]. The more reliable Heyd–Scuseria–Ernzerhof (HSE06) hybrid function is also applied to verify the band structure[48]. The projector augmented wave method is adopted to represent the ion–electron interactions[49, 50], 400 eV is considered as the energy cutoff. The conjugate gradient algorithm is used to fully optimize the crystal structure to the ground state until the energy and force convergence criteria reach 10^{-7} eV and 1 meV/Å, respectively, while a vacuum length of 25 Å is chosen to ensure a true 2D system. K-point meshes are set as 15 × 15 × 1 and 30 × 30 × 1 to obtain the energy band and the MAE, respectively. The density function perturbation theory method implemented in Phonopy code is used to calculate phonon spectra along high symmetry lines[51]. To obtain MAE, we calculate the spin orbit coupling (SOC) by including it in the complete k-point grid (i.e., 900 K points in total). The charge doping simulation is performed by injecting electrons/holes into the system. A 16 × 16 × 1 supercell is selected and a Monte Carlo simulation[52] based on the 2D Ising model is used to calculate the Curie temperature.

2.1. Geometric structures and stabilities

The Ir_2TeI_2 monolayer is homogeneous to one of the layers of the M_2ZX_2-type van der Waals(vdW) layered telluride Ln_2TeI_2 (Ln = La, Gd)[53]. The crystal structure of Ir_2TeI_2 is highlighted in Fig. 1(a) and belongs to the P3m1 space group. The octahedral metal center atom Te and I atoms separate these layers, forming three densely packed I-Ir-Te-Ir-I plates in the cell. The structure optimization shows that the lattice constant of Ir_2TeI_2 is $a = b$ = 4.02 Å. The stability of the structure can be checked by estimating the cohesion energy $E_{coh} = (E_{Ir_2TeI_2} - 2E_{Ir} - E_{Te} - 2E_I)/5$, where E_{Ir}, E_{Te}, E_I and $E_{Ir_2TeI_2}$ are the energies corresponding to their subscripts, respectively. For example, E_{Ir} is the total energy of the Ir atom. The obtained cohesion energy of –3.054 eV/atom, which is slightly smaller than that of graphene (–7.85 eV/atom). The powerful cohesion energy favors strong binding effect and the possibility of experimental synthesis of basic materials.

To verify the dynamic stability, we calculated the phonon spectrum of the Ir_2TeI_2 and no appreciable imaginary phonon modes are observed, indicating that this lattice is dynamical stable, as shown in Fig. 1(c). Experimentally, the synthesis and mechanical peeling of 2D vdW materials are an ideal technology to realize a single-layer structure[54, 55]. To evaluate its peelability, the interlayer interactions were examined. Therefore, the exfoliation energy is predicted by simulating the exfoliation process of the M_2ZX_2 type layered tellurium halide, as plotted in Fig. 1(d). The calculation finds that the exfoliation energy is 1.24 J/m^2, which is lower than that of Mxenes[56–58]. Therefore, it is expected that the room temperature Ir_2TeI_2 monolayer can be acquired by bulk exfoliation, which demonstrates the feasibility of experimental synthesis.

We have also investigated the mechanical properties of Ir_2TeI_2 and calculated the elastic constants: c_{11} = 200.7 N/m, c_{22} = 197.2 N/m, c_{12} = 55.6 N/m, c_{66} = 17.98 N/m, which meet the Bonn criterion: $c_{66} > 0$, $c_{11}c_{22} - c_{12}^2 > 0$[59]. According to the elastic constant, the in-plane Young's modulus $Y(\phi)$ and Poisson's ratio $V(\theta)$ could be calculated along any direction by[60]:

$$Y(\theta) = \frac{c_{11}c_{22} - c_{12}^2}{c_{11}\sin^4\theta + A\sin^2\theta\cos^2\theta + c_{22}\cos^4\theta}, \quad (1)$$

$$V(\theta) = \frac{c_{12}\sin^4\theta + B\sin^2\theta\cos^2\theta + c_{12}\cos^4\theta}{c_{11}\sin^4\theta + A\sin^2\theta\cos^2\theta + c_{22}\cos^4\theta}, \quad (2)$$

where $A = c_{11}c_{22} - c_{12}^2/c_{66} - 2c_{12}$, $B = c_{11} + c_{22} - \left(c_{11}c_{22}c_{12}^2\right)/c_{66}$. $\theta = 0°$ corresponds to the x axis, Figs. 1(e) and 1(f) show the results of $Y(\theta)$ and $V(\theta)$ related to angle. The Young's modulus of Ir_2TeI_2 ranges from 78.1–83.2 N/m, which is higher than that of silicon[61] (62 N/m) and lower than that of graphene (340 N/m)[62]; indicating that the structure has mechanical flexibility moderate and hardness, thus proving the feasibility of tuning the magnetic order by applying strain. The Poisson's ratio is between 0.24 and 0.28, which is within the reasonable range suggested by Gao *et al.*[63]. This indicates that its moderate structural response to external forces also facilitates the achievement of strain control.

2.2. Electronic band structures

After determining the stability, we investigate its electronic and magnetic properties. Figs. 2(a) and 2(b) show the electronic energy band structures of Ir_2TeI_2 and the partial density of states (PDOS) for the distinguished spin channel of Ir atoms, respectively. It has an insulating state in the spin-down channel and a metallic state in the spin-up channel, thus possessing intrinsic half-metallic properties. The band gap of the spin-down channel is up to 1.29 eV (As shown in Fig. S1, the HSE is 1.62 eV that more than PBE 0.3 eV), which is sufficient to prevent hot spin flipping. Due to the strong spinpolarization at the fermi level, 100% spin filter efficiency can be maintained over a wide range of positive or negative bias of about 0.5 V. This makes Ir_2TeI_2 an attractive candidate for spin injection.

2.3. Magnetic properties

The FM state of Ir_2TeI_2 exhibits an integer magnetic moment of 2 μB per unit cell, mainly contributed by two equivalent Ir atoms in the unit cell. the magnetization of Ir ions can be well understood by the electron local function and spin charge density (given in Figs. S2(a) and S2(b)), only a few spin-polarized electrons are located around the Ir ion, thus resulting in a magnetic moment of 1.0 μ_B/Ir. The FM coupling of Ir_2TeI_2 monolayers can be well understood by the competition between direct exchange and superexchange of Ir atoms mediated by Te and I atoms. To verify the magnetic ground state, we build the supercell to evaluate the relative stability of FM and AFM states, so we construct FM and three possible AFM configurations; as illustrated in Fig. 3(a). The total en-

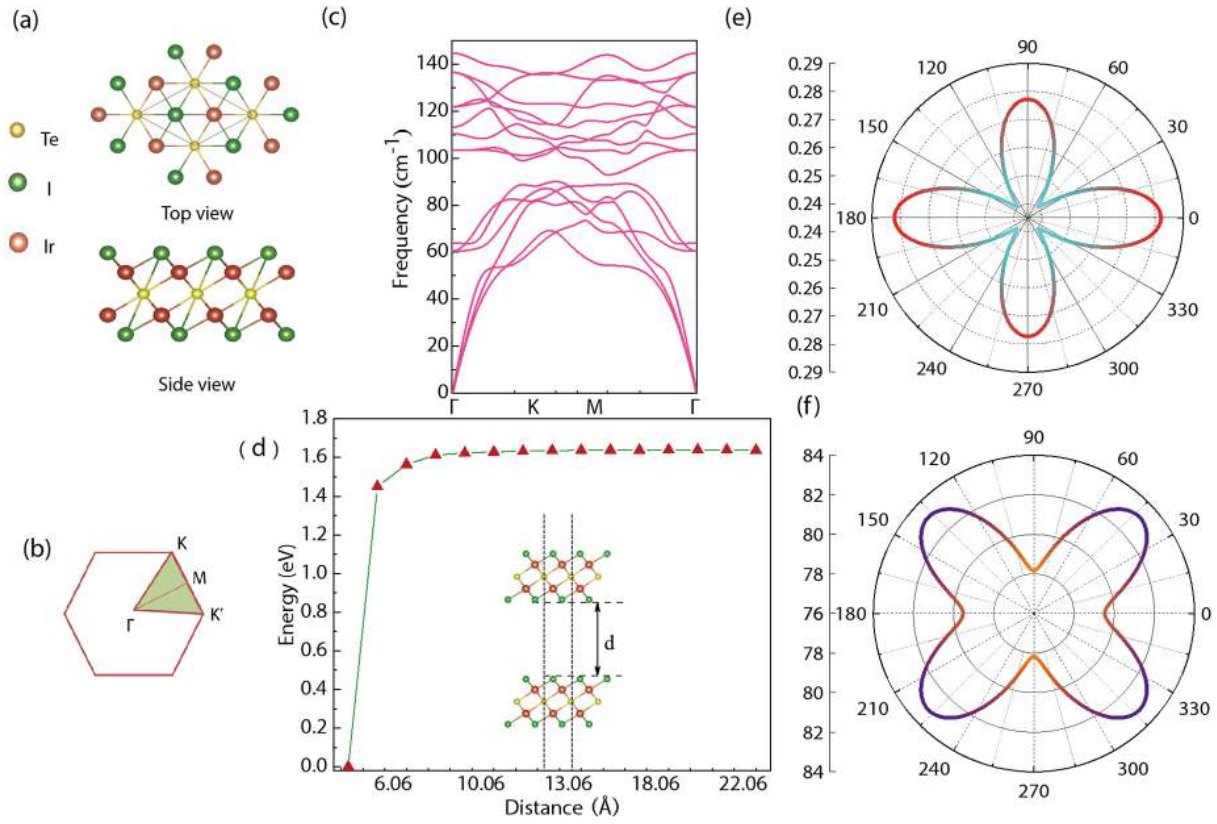

Fig. 1. (Color online) (a) Lattice structure of Ir_2TeI_2 monolayer. (b) Diagram of the first Brillouin zone of 2D hexagonal structure. (c) The phonon dispersion of Ir_2TeI_2. (d) The energy change when Ir_2TeI_2 monolayer is stripped. *d* is the distance between the two layers. (e, f) Graphs of Poisson's ratio and Young's modulus, respectively.

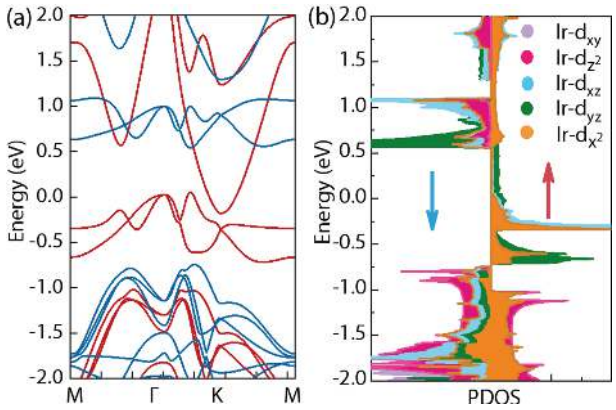

Fig. 2. (Color online) (a) Electron band structure of Ir_2TeI_2 monolayer, the red represents spin up, blue represents spin down. (b) The PDOS of Ir atom in different spin channels.

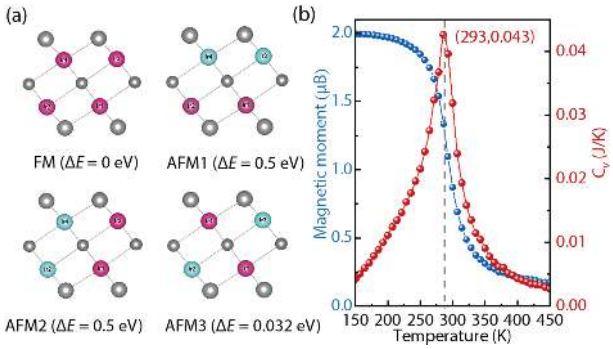

Fig. 3. (Color online) (a) FM and three types of AFM magnetic order diagrams of magnetic atoms, purple and blue represent different spin orientations, respectively. Δ*E* represents the energy of different magnetic sequences with respect to the FM state. (b) The change of specific heat and magnetism relative to temperature, red line denotes specific heat C_v and blue denotes atomic mean magnetic moment.

ergy calculation proves that FM coupling is more energy stable than AFM coupling. According to Goodstoy-Kanamori-Anderson (GKA) rule[64], FM coupling is suitable for 90° superexchange interaction between two magnetic ions, while AFM coupling is more suitable for 180° superexchange interaction. Therefore, the total exchange interaction in the monolayer is dominated by FM superexchange.

According to Mermin-Wagner's theorem[8], MA is crucial for establishing 2D ferromagnetism over long distances. MAE characterizes the degree of difficulty of the total magnetization axis, which is evaluated by considering the magnetization direction function of the total energy of SOC. After completing the convergence test of K point and energy cutoff, as shown in Figs. S3 and S4, the MAE per unit cell (uc) calculation of different crystal axes is carried out. The data is given in Table 1, which shows high magnetic anisotropy. This indicates that the structure has the potential to be applied in magnetic storage devices.

Due to the strong MA and the magnetic axis along the out-of-plane, based on the Ising model, the T_c of the 2D ferromagnet is calculated by using Monte Carlo (MC) simulation. Here, the Hamiltonian equation is given as:

$$H = -\sum_{\langle i,j\rangle} J_1 m_i m_j - \sum_{\langle\langle i,j\rangle\rangle} J_2 m_i m_j, \quad (3)$$

Table 1. MAE (meV) of unit cell with respect to (001) direction, anisotropy constant K (meV) and T_c (K)

Magnetic axis	001	001	110	111	T_c	K_1	K_2
ΔE (meV/uc)	1.024	0	1.016	0.582	293	0.33	0.176

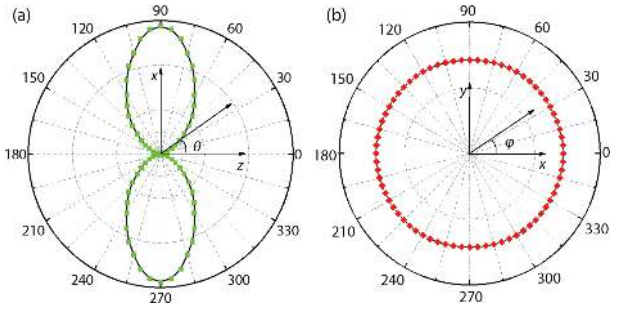

Fig. 4. (Color online) Angle dependence of MAE of Ir_2TeI_2 in (a) xz plane and (b) xy plane, where θ and φ correspond to the z and x axes, respectively.

$$E_{FM} = E_0 - 6J_1M^2 - 12J_2M^2,$$

$$E_{AFM1} = E_0 + 6J_1M^2 - 12J_2M^2,$$

$$E_{AFM2} = E_0 - 2J_1M^2 + 4J_2M^2,$$

$$E_{AFM3} = E_0 + 2J_1M^2 + 4J_2M^2. \quad (4)$$

In Eq. (3), J_1 and J_2 are the nearest neighbor and second neighbor exchange coupling parameters, respectively, which is extracted from the energy difference between FM state and AFM state. m_i is the spin vector of Ir atom. We use the equations above to fit the nearest-neighbor exchange interaction, we have J_1 = 17.8 meV and the second-nearest-neighbor exchange interaction J_2 = 3 meV are both positive, which also prove that the Ir_2TeI_2 prefers the FM state. Average magnetic moment (m) and specific heat (C_v) results are plotted in Fig. 3(b), the T_c is extracted from the phase transition point from FM to the paramagnetic state at about 293 K, which may be beyond the room temperature magnetic applications.

Based on the symmetry of a uniaxial quadrilateral of a 2D system, the angle dependence of MAE[65] can be described as:

$$\mathrm{MAE}(\theta) = K_1\sin^2\theta + K_2\sin^4\theta. \quad (5)$$

In Eq. (5), K_1 and K_2 are the anisotropic constants associated with the system and θ is the azimuth angle of rotation. The positive values of both K_1 and K_2 indicate that the structure has a strong Ising ferromagnetism with the magnetization direction parallel to the z-axis, while $K_1 < 0$ indicates an in-plane magnetization axis. As shown in Table 1, K_1 and K_2 of Ir_2TeI_2 are both positive, belonging to the 2D Ising family. MAE reaches the maximum value of 0.5 meV/Ir at $\theta_{xz} = \theta_{yz} = \pi/2$. Figs. 4(a) and 4(b) give the variation of MAE in the xz and xy planes as the rotation axis rotates, respectively. The MAE is strongly correlated with the azimuthal angle (θ), while the dependence on the polarity angle (φ) is extremely small, which again confirms the strong MA of the Ir_2TeI_2 monolayer. Therefore, it can be inferred that a large MAE is sufficient to stabilize the ferromagnetism and thus resist thermal fluctuations at a specific temperature.

2.4. Magnetic controlling

Low-dimensional materials generally exhibit a sensitive response to external stimuli, which allows their electronic or magnetic properties to be adjusted. For example, through the orbital occupation caused by charge doping in the Fe/graphene complex system, the MAE value and the orientation of the easy axis of magnetization have been successfully adjusted[66]. Jiang *et al.*[38] have reported that it is possible to introduce carrier doping into 2D CrI_3 through an electronic gate that controls magnetism.

Here, we observe that the MAE of Ir_2TeI_2 can be significantly tuned via charge doping, meanwhile the orientation of the easily magnetized axis can be switched. The calculated results are plotted in Fig. 5(a). It can be seen that under different magnetization directions, the total energy changes with the change of the carrier concentration (n). Under electronic doping ($n < 0$), the energy difference between out-of-plane and in-plane magnetization decreases with the increase of electronic doping. When $n < -0.44 \times 10^{18}$ m^{-2}, Ir_2TeI_2 transforms into in-plane magnetization. In contrast, hole doping ($n > 0$) maintains the out-of-plane magnetization within a certain range and increases the doping concentration, which could transform it into in-plane magnetization. The critical concentration of hole doping is higher than 2.56×10^{18} m^{-2}. Experimentally, it is effective to make the carrier concentration of 10^{17}–10^{18} m^{-2} in a 2D system, Therefore, carrier doping can be an effective way to regulate ferromagnetism.

Strain modulation is a flexible method for tuning the electronic properties of 2D layered structures. It can change the bond angles and distance between atoms to affect the interaction between atoms, resulting in the change of electronic properties. Lv *et al.*[67] have proven that the switching of the FM order can be controlled by strain as an inducer. Here, we find that the transition of FM state and AFM state in Ir_2TeI_2 monolayer can also be controlled by biaxial strain. When tensile strain is applied, as is illustrated in Fig. 6(d), the magnetic order tends to be AFM; whereas when compressive strain is applied, the structure is in FM state. It is worth noting that the MAE of Ir_2TeI_2 monolayer will further increase and the band gap of spin-down will narrow as the compression stress decreases, as is shown in Fig. 6(c).

The behavior transformation of intrinsic FM half-metal Ir_2TeI_2 monolayer under stress can be understood by the competition between two different exchange interactions. For a general 2D magnetic structure, the direct exchange interaction between magnetic atoms (represented by JD) will result in the AFM state, while the superexchange interaction between magnetic atoms (represented by JS) will contribute to the FM state with the same spin orientation. The magnetic state of Ir_2TeI_2 monolayer is jointly determined by JD + JS, where JD and JS are negative and positive, respectively. For Ir_2TeI_2 monolayer in ground state without strain, |JD| is less than JS; therefore, the system exhibits FM properties. As mentioned above, when compressive strain is applied, as shown in Fig. 6(a), the distance between Ir1-Ir2 increases, so the direct exchange effect weakens; that is, |JD| decreases. Correspondingly, the Ir1-Te-Ir2 distance decreases, so the superex-

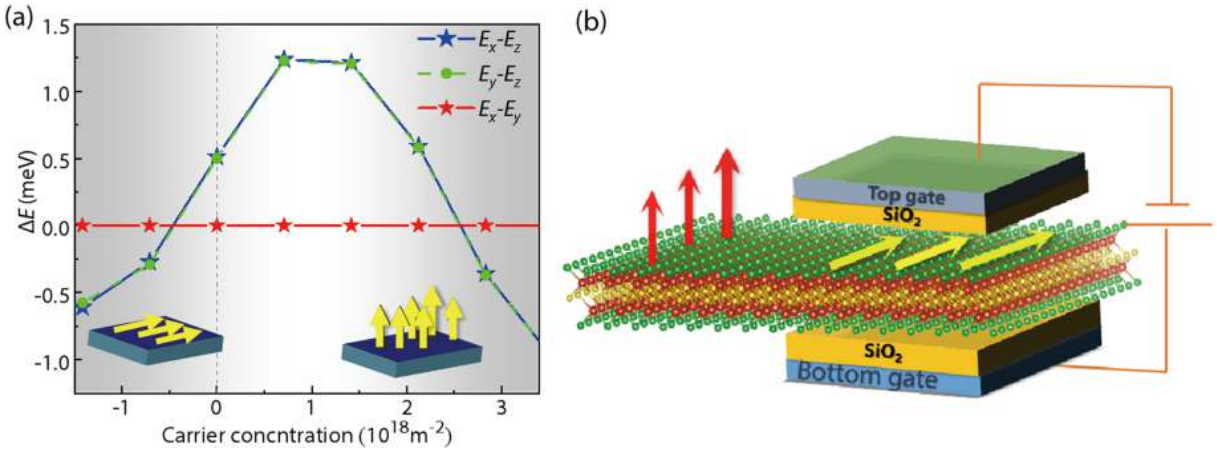

Fig. 5. (Color online) (a) Carrier injection regulates the magnetization direction in ferromagnetic state. (b) A schematic diagram of a 2D magnetoelectric device controlled by electrostatic doping to achieve the giant magnetoresistance effect, the 2D FM monomolecular layer is bi-gated, while the two by like SiO_2 dielectric layers act to avoid direct tunneling.

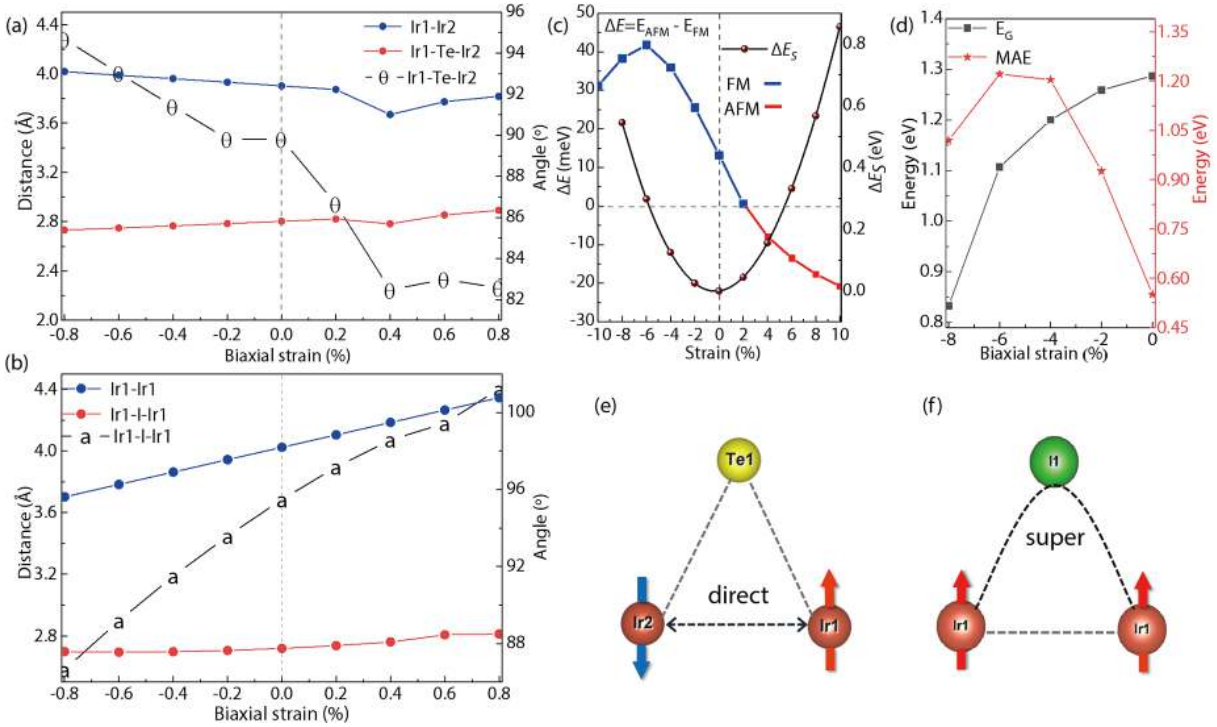

Fig. 6. (Color online) (a) The variation of bond lengths of the closest neighbors Ir1-Ir2 and Ir-Te between layers and bond angle β as a function of strain. (b) The variation of bond lengths of the next closest neighbors Ir1-Ir1 and Ir-I within layers and bond Angle α as a function of strain. (c) Structural energy changes and competition between FM and AFM under strain (–10% to 10%). (d) The value change of band gap and MAE with compressive strain. (e) The antiferromagnetic coupling of direct exchange between magnetic atoms and (f) the ferromagnetic coupling of hyperexchange mediated by Te/I atoms.

change interaction increases; that is, JS increases, so there is still JD + JS > 0 and increase, which means that the FM state is enhanced.

In the same way, for the next neighbor atoms in the same layer with weaker exchange effect, as shown in Fig. 6(b), its JS increases and JD decreases, so JS + JD is a small negative value, which will result in a weak AFM state. Since the influence of the exchange interaction between the nearest neighbor magnetic atoms is much greater than that of the next neighbor atoms, on the whole, the compressive stress will lead to a stronger FM state. When the strain approaches 2%, the bond angle is close to 90° and reaches the critical point of magnetic order transition. At this time, JS is equal to |JD| and JD + JS = 0. Similarly, when the strain is greater than 2%, the nearest neighbor |JD| between layers increases and JS decreases, so the magnetic order orientation of the structure is an AFM state. Conversely, changes in the same layer lead to FM state but interlayer JD prioritize the determination of magnetism, with JD+JS < 0, so the Ir_2TeI_2 monolayer transforms to the AFM state. These results demonstrate that strain is an effective method to regulate the magnetic and electrical properties of monolayers and also provides a potential candidate material for future nanoelectronic applications, which is worthy of further study in the experiment.

3. Conclusions

In summary, we computationally predicted a stable half-metal Ir_2TeI_2 monolayer, where the ground state exhibits intrinsic FM properties and strong MAE. The T_c is estimated to be 293 K, which is higher than that reported for 2D CrI_3 and $Cr_2Ge_2Te_6$ crystals, the bands are spin-polarized with a spin-down band gap of 2.9 eV, sufficient to prevent thermal inversion. The analysis of the MAE demonstrated that the structure is easy to be magnetized outside the plane and the MAE is up to 0.5 meV/Ir. The doping of holes and electrons can switch the magnetization axis between the in-plane and out-plane directions, which can effectively control the spin injection/detection in the 2D structure. In addition, we find that biaxial strain can induce the conversion of the states of FM and AFM. Under tensile strain, the AFM order tends to be stable. However, under compressive strain, the FM order is further stable, the half-metal properties are maintained and the MAE is increased. Our results provide potential candidates for future applications of functional nanoelectrons and are worthy of further study.

Acknowledgements

This work is supported by the Taishan Scholar Program of Shandong Province (No. ts20190939), National Natural Science Foundation of China (Grant No. 62071200, 12004137, 11804116, 52173283), the Natural Science Foundation of Shandong Province (Grant No. ZR2018MA035, ZR2020QA052, ZR2019MA041), Independent Cultivation Program of Innovation Team of Jinan City (Grant No. 2021GXRC043).

Appendix A. Supplementary materials

Supplementary materials to this article can be found online at https://doi.org/10.1088/1674-4926/43/5/052001.

References

[1] Huang B, Clark G, Navarro-Moratalla E, et al. Layer-dependent ferromagnetism in a van der Waals crystal down to the monolayer limit. Nature, 2017, 546, 270
[2] Gong C, Li L, Li Z L, et al. Discovery of intrinsic ferromagnetism in two-dimensional van der Waals crystals. Nature, 2017, 546, 265
[3] Deng Y J, Yu Y J, Song Y C, et al. Gate-tunable room-temperature ferromagnetism in two-dimensional Fe_3GeTe_2. Nature, 2018, 563, 94
[4] Bonilla M, Kolekar S, Ma Y J, et al. Strong room-temperature ferromagnetism in VSe_2 monolayers on van der Waals substrates. Nat Nanotechnol, 2018, 13, 289
[5] O'Hara D, Zhu T C, Trout A H, et al. Room temperature intrinsic ferromagnetism in epitaxial manganese selenide films in the monolayer limit. Nano Lett, 2018, 18, 3125
[6] Zheng S, Huang C, Yu T, et al. High-temperature ferromagnetism in an Fe_3P monolayer with a large magnetic anisotropy. J Phys Chem Lett, 2019, 10, 2733
[7] Lee J U, Lee S, Ryoo J H, et al. Ising-type magnetic ordering in atomically thin $FePS_3$. Nano Lett, 2016, 16, 7433
[8] Mermin N D, Wagner H. Absence of ferromagnetism or antiferromagnetism in one- or two-dimensional isotropic Heisenberg models. Phys Rev Lett, 1966, 17, 1133
[9] Stöhr J, Siegmann H C. Polarized electrons and magnetism. Magnetism: From Fundamentals to Nanoscale Dynamics. Nanoscale Dynamics, 2006, 313
[10] Lado J L, Fernández-Rossier J. On the origin of magnetic anisotropy in two dimensional CrI_3. 2D Mater, 2017, 4, 035002
[11] Xu C S, Feng J S, Xiang H J, et al. Interplay between Kitaev interaction and single ion anisotropy in ferromagnetic CrI_3 and $CrGeTe_3$ monolayers. npj Comput Mater, 2018, 4, 57
[12] Li X X, Dong B J, Sun X D, et al. Perspectives on exfoliated two-dimensional spintronics. J Semicond, 2019, 40, 081508
[13] Wang X, Tang J, Xia X X, et al. Current-driven magnetization switching in a van der Waals ferromagnet Fe_3GeTe_2. Sci Adv, 2019, 5, eaaw8904
[14] Ikeda S, Miura K, Yamamoto H, et al. A perpendicular-anisotropy CoFeB–MgO magnetic tunnel junction. Nat Mater, 2010, 9, 721
[15] Dieny B, Chshiev M. Perpendicular magnetic anisotropy at transition metal/oxide interfaces and applications. Rev Mod Phys, 2017, 89, 025008
[16] Katmis F, Lauter V, Nogueira F S, et al. A high-temperature ferromagnetic topological insulating phase by proximity coupling. Nature, 2016, 533, 513
[17] Liu L, Ren X, Xie J H, et al. Magnetic switches via electric field in BN nanoribbons. Appl Surf Sci, 2019, 480, 300
[18] Wu Z, Yu J, Yuan S. Strain-tunable magnetic and electronic properties of monolayer CrI_3. Phys Chem Chem Phys, 2019, 21, 7750
[19] Ohno H, Chiba D, Matsukura F, et al. Electric-field control of ferromagnetism. Nature, 2000, 408, 944
[20] Weisheit M, Fähler S, Marty A, et al. Electric field-induced modification of magnetism in thin-film ferromagnets. Science, 2007, 315, 349
[21] Wang Z R, Hao Z, Wang X J, et al. Cytokine storm biomarkers: A flexible and regenerative aptameric graphene–nafion biosensor for cytokine storm biomarker monitoring in undiluted biofluids toward wearable applications. Adv Funct Mater, 2021, 31, 2170026
[22] Wang Z R, Hao Z, Yu S F, et al. An ultraflexible and stretchable aptameric graphene nanosensor for biomarker detection and monitoring. Adv Funct Mater, 2019, 29, 1905202
[23] Wang Y P, Ji W X, Zhang C W, et al. Discovery of intrinsic quantum anomalous Hall effect in organic Mn-DCA lattice. Appl Phys Lett, 2017, 110, 233107
[24] Zhang L, Zhang S F, Ji W X, et al. Discovery of a novel spin-polarized nodal ring in a two-dimensional HK lattice. Nanoscale, 2018, 10, 20748
[25] Zhang M H, Chen X L, Ji W X, et al. Discovery of multiferroics with tunable magnetism in two-dimensional lead oxide. Appl Phys Lett, 2020, 116, 172105
[26] Huang C X, Feng J S, Wu F, et al. Toward intrinsic room-temperature ferromagnetism in two-dimensional semiconductors. J Am Chem Soc, 2018, 140, 11519
[27] You J Y, Zhang Z, Dong X J, et al. Two-dimensional magnetic semiconductors with room Curie temperatures. Phys Rev Research, 2020, 2, 013002
[28] Yu J X, Zang J. Giant perpendicular magnetic anisotropy in Fe/III-V nitride thin films. Sci Adv, 2018, 4, eaar7814
[29] Jiang S W, Shan J, Mak K F. Electric-field switching of two-dimensional van der Waals magnets. Nat Mater, 2018, 17, 406
[30] You J Y, Zhang Z, Gu B, et al. Two-dimensional room temperature ferromagnetic semiconductors with quantum anomalous Hall effect. arXiv: 1904.11357, 2019
[31] Novoselov K S. Nobel lecture: Graphene: Materials in the flatland. Rev Mod Phys, 2011, 83, 837
[32] Yang S W, Peng R C, Jiang T, et al. Non-volatile 180° magnetization reversal by an electric field in multiferroic heterostructures. Adv Mater, 2014, 26, 7091
[33] Kum H S, Lee H, Kim S, et al. Heterogeneous integration of single-crystalline complex-oxide membranes. Nature, 2020, 578, 75
[34] Caretta L, Rosenberg E, Büttner F, et al. Interfacial Dzyaloshinskii-Moriya interaction arising from rare-earth orbital magnetism in insulating magnetic oxides. Nat Commun, 2020, 11, 1090
[35] Cui Q R, Liang J H, Shao Z J, et al. Strain-tunable ferromagnetism

and chiral spin textures in two-dimensional Janus chromium dichalcogenides. Phys Rev B, 2020, 102, 094425
[36] Dong X J, You J Y, Gu B, et al. Strain-induced room-temperature ferromagnetic semiconductors with large anomalous hall conductivity in two-dimensional $Cr_2Ge_2Se_6$. Phys Rev Appl, 2019, 12, 014020
[37] Saito Y, Nojima T, Iwasa Y. Highly crystalline 2D superconductors. Nat Rev Mater, 2017, 2, 16094
[38] Jiang S W, Li L Z, Wang Z F, et al. Controlling magnetism in 2D CrI_3 by electrostatic doping. Nat Nanotechnol, 2018, 13, 549
[39] Abdollahi M, Bagheri Tagani M. Tuning intrinsic ferromagnetic and anisotropic properties of the Janus VSeS monolayer. J Mater Chem C, 2020, 8, 13286
[40] Zhang S J, Zhang C W, Zhang S F, et al. Intrinsic Dirac half-metal and quantum anomalous Hall phase in a hexagonal metal-oxide lattice. Phys Rev B, 2017, 96, 205433
[41] Yang H X, Vu A D, Hallal A, et al. Anatomy and giant enhancement of the perpendicular magnetic anisotropy of cobalt – graphene heterostructures. Nano Lett, 2016, 16, 145
[42] Ma A N, Wang P J, Zhang C W. Intrinsic ferromagnetism with high temperature, strong anisotropy and controllable magnetization in the CrX (X = P, As) monolayer. Nanoscale, 2020, 12, 5464
[43] Bafekry A, Neek-Amal M, Peeters F M. Two-dimensional graphitic carbon nitrides: Strain-tunable ferromagnetic ordering. Phys Rev B, 2020, 101, 165407
[44] Kresse G, Furthmüller J. Efficiency of ab-initio total energy calculations for metals and semiconductors using a plane-wave basis set. Comput Mater Sci, 1996, 6, 15
[45] Kresse G, Furthmüller J. Efficient iterative schemes for *ab initio* total-energy calculations using a plane-wave basis set. Phys Rev B, 1996, 54, 11169
[46] Perdew J P, Burke K, Ernzerhof M. Generalized gradient approximation made simple. Phys Rev Lett, 1996, 77, 3865
[47] Wang L, Maxisch T, Ceder G. Oxidation energies of transition metal oxides within the GGA+U framework. Phys Rev B, 2006, 73, 195107
[48] Krukau A V, Vydrov O A, Izmaylov A F, et al. Influence of the exchange screening parameter on the performance of screened hybrid functionals. J Chem Phys, 2006, 125, 224106
[49] Blöchl P E. Projector augmented-wave method. Phys Rev B, 1994, 50, 17953
[50] Kresse G, Joubert D. From ultrasoft pseudopotentials to the projector augmented-wave method. Phys Rev B, 1999, 59, 1758
[51] Togo A, Oba F, Tanaka I. First-principles calculations of the ferroelastic transition between rutile-type and $CaCl_2$-typeSiO_2 at high pressures. Phys Rev B, 2008, 78, 134106
[52] Liu J, Sun Q, Kawazoe Y, et al. Exfoliating biocompatible ferromagnetic Cr-trihalide monolayers. Phys Chem Chem Phys, 2016, 18, 8777
[53] Ryazanov M, Simon A, Mattausch H. La_2TeI_2: a new layered telluride iodide with unusual electrical properties. Inorg Chem, 2006, 45, 10728
[54] Jayasena B, Subbiah S. A novel mechanical cleavage method for synthesizing few-layer graphenes. Nanoscale Res Lett, 2011, 6, 95
[55] Nicolosi V, Chhowalla M, Kanatzidis M G, et al. Liquid exfoliation of layered materials. Science, 2013, 340, 1226419
[56] He J J, Lyu P B, Nachtigall P. New two-dimensional Mn-based MXenes with room-temperature ferromagnetism and half-metallicity. J Mater Chem C, 2016, 4, 11143
[57] Gao G, Ding G, Li J, et al. Monolayer MXenes: Promising half-metals and spin gapless semiconductors. Nanoscale, 2016, 8, 8986
[58] Hu L, Wu X J, Yang J L. Mn_2C monolayer: A 2D antiferromagnetic metal with high Néel temperature and large spin–orbit coupling. Nanoscale, 2016, 8, 12939
[59] Mouhat F, Coudert F X. Necessary and sufficient elastic stability conditions in various crystal systems. arXiv: 1410.0065, 2014
[60] Cadelano E, Palla P L, Giordano S, et al. Elastic properties of hydrogenated graphene. Phys Rev B, 2010, 82, 235414
[61] Ding Y, Wang Y L. Density functional theory study of the silicene-like SiX and XSi_3 (X = B, C, N, Al, P) honeycomb lattices: The various buckled structures and versatile electronic properties. J Phys Chem C, 2013, 117, 18266
[62] Andrew R C, Mapasha R E, Ukpong A M, et al. Mechanical properties of graphene and boronitrene. Phys Rev B, 2012, 85, 125428
[63] Gao Z B, Dong X, Li N B, et al. Novel two-dimensional silicon dioxide with in-plane negative poisson's ratio. Nano Lett, 2017, 17, 772
[64] Weiss A. John B. Goodenough: Magnetism and the chemical bond. Berichte Der Bunsengesellschaft Für Physikalische Chemie, 1964, 68, 996
[65] Hajalilou A, Hashim M, Mohamed Kamari H. Structure and magnetic properties of $Ni_{0.64}Zn_{0.36}Fe_2O_4$ nanoparticles synthesized by high-energy milling and subsequent heat treatment. J Mater Sci Mater Electron, 2015, 26, 1709
[66] Gong S J, Duan C G, Zhu Z Q, et al. Manipulation of magnetic anisotropy of Fe/graphene by charge injection. Appl Phys Lett, 2012, 100, 122410
[67] Lv H Y, Lu W J, Shao D F, et al. Strain-controlled switch between ferromagnetism and antiferromagnetism in 1T –CrX_2 (X = Se, Te) monolayers. Phys Rev B, 2015, 92, 214419

Didi Zhao received her B.Sc. degree in physics from the University of Jinan, China. She is now a physics master's student in the Spintronics team at the School of Physics, University of Jinan. Her main research fields are spintronics and the topological properties of low dimensional materials.

Peiji Wang earned his B.Sc. degree in physics from the Jilin University in 1987. He received his Ph.D. degree in optics from the Harbin Institute of Technology in 2009. He has been working at the University of Jinan since 1987. His current research focuses on semiconductor materials, nanomaterial design and the tuning of topological materials.